Model and Control of a Flap System Mitigating Wind Impact on Structures

Maria Boberg, Glauco Feltrin and Alcherio Martinoli

Abstract— In this work, we investigate a model-based control for a flap system aiming at mitigating wind-induced vibrations of long-span bridges. Our contribution is threefold: first, we developed an integrated flap system able to control a bridge section model; second, we proposed a model able to properly capture the nonlinear interaction between wind and the structure; third, we optimized a linear control law for the flap position able to robustly cope with the nonlinear forces exerted on the flap. The model accuracy and the system performance were systematically validated by wind tunnel experiments.

I. INTRODUCTION

Long-span bridges are particularly vulnerable to wind loads, owing to their inherently low structural damping, low natural frequencies, and adjacent fundamental torsional and vertical mode frequencies. This leads to wind-induced instabilities, causing potential damage to the whole structure.

Most solutions for this problem deployed on real bridges consist of passive elements that reduce the aerodynamic requirements on the cross-section [1]. However, a passive solution cannot adapt to dynamic wind conditions. Active solutions could potentially lead to a more favorable performance/cost trade-off in the building and maintenance phases as well as new opportunities for improving bridge aesthetics.

One possible active solution is to install multiple mobile flaps along the bridge girder in order to alter its aerodynamic profile, enabling stabilizing forces on the structure, a concept illustrated in Fig. 1. Furthermore, the angular position of the adjustable flaps is controlled as a function of the wind field and/or the displacement of the structure whose dynamic state can be measured with an underlying sensor network.

Although several control strategies for damping bridge deck oscillations, in particular the flutter phenomenon, have been investigated, only two research groups have provided experimental validation of active bridge flutter control. Kobayashi and Nagaoka managed to increase the wind speed at which flutter occurs by 50% [2]. Hansen was also able to increase the flutter velocity with active control using a new bridge section model design (larger scale, and different flap placement) [3]. Both research groups used bridge section models endowed with a single flap on each side of the girder.

We aim to extend the investigation of active flutter control to bridge section models endowed with multiple flaps, such

Maria Boberg and Alcherio Martinoli are with the Distributed Intelligent Systems and Algorithms Laboratory, School of Architecture, Civil and Environmental Engineering, École Polytechnique Fédérale de Lausanne, Switzerland. `maria.boberg@epfl.ch` and `alcherio.martinoli@epfl.ch`

Maria Boberg and Glauco Feltrin are with the Structural Engineering Laboratory, Swiss Federal Laboratories for Materials Science and Technology, Duebendorf, Switzerland. `glauco.feltrin@empa.ch`

that distributed control strategies can be studied and validated experimentally. Towards this goal, we have focused on the mechatronic design and control of a single flap. A core challenge for an effective control law design, is to properly capture the nonlinear, noisy wind force exerted on the flap.

Neither Kobayashi nor Hansen, who aimed to investigate the feasability of active flutter control using flaps, directly addressed the issue of position control of a single flap. When designing the flutter control they both employed a model introduced by Kobayashi: essentially two coupled linear differential equations (of the bridge deck and flap displacements and their time derivatives) based on the wing-aileron-tab configuration model developed by Theodorsen and Garrick [4]. However, the model assumptions (e.g., no flow influence of upwind elements on downwind elements) are strong and their theoretical results did not match experimental data well.

Fowler and D'Andrea performed wind tunnel experiments researching aircraft flight formation [5]. They employed a manually tuned linear control law for the flap actuation. The flap angle was controlled in an open-loop fashion by a servo motor, while the control signal to the servo motor was generated in a closed-loop fashion taking into account the yaw and roll of the airfoil. The dynamic response of the system to the control input was captured by a fourth-order state-space model. However, they did not model the actual underlying physical mechanism of the interaction between the flap and the surrounding wind field.

In this work, we propose a model-based approach, well-anchored to physical reality, allowing for fine tuning of a linear control law and its corresponding parameters. Not only does the model-based approach provide a safe control tuning environment, but also a flexible and fast platform for testing
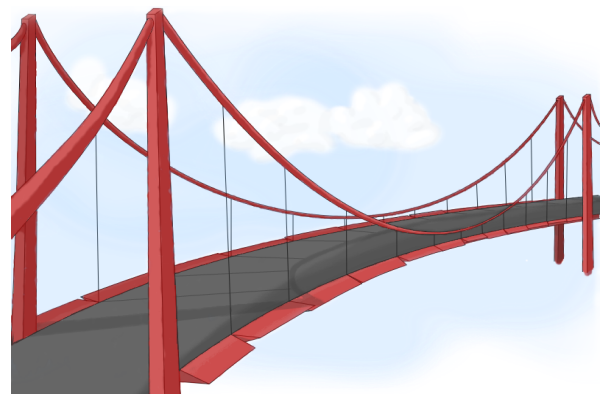

Fig. 1. Conceptual figure of the multi-flap wind mitigation strategy.

new control laws. Furthermore, a method for identifying the model parameters from experimental data is proposed, and the approach is validated with our prototype flap in a wind tunnel. The model was developed in Matlab Simulink®.

Our proposed model can be extended to include the bridge deck dynamics, and Kobayashi's model is a good starting point. However, this is not within the scope of this paper.

II. MATERIAL AND METHODS

In order to investigate the control of the flap, we designed a dedicated test rig, as seen in Fig. 2(a). The flap prototype is made of ABS plastic and was manufactured using a 3D printer; the design is symmetric (width: 400 mm, chord length: 134 mm, max thickness: 49 mm) and both motor and driver fit inside, as seen in Fig. 2(b). In our setup we used a 20W DC motor with graphite brushes (model: 118751), gear reduction rate of 53:1 (model: 144035) optical encoder (model: 225778), and a digital positioning controller (model: 390003), all from Maxon Motor Inc. The manufacturer provides an auto-tuning function that allows quick tuning of the motor control parameters (proportional, integral, and derivative coefficients). The tuning criterion can be set between a hard and a soft response, however, full tuning transparency is not provided. Running the auto-tuning procedure for the control parameters when the motor is placed inside the flap is possible. However, even when the flap is subjected to low wind speeds, the software aborts the tuning operation due to the nonsteady forces. Therefore, in this paper whenever auto-tuned parameters are mentioned, they were tuned with the flap mounted, but without wind.

The motor's speed and torque requirements were based on approximate calculations and previous work within this field. The required flap speed depends on the motion of the bridge deck it controls since it will probably move at the same frequency, but with a different amplitude. The flap in Hansen's experimental setup moved at a frequency of 1.5
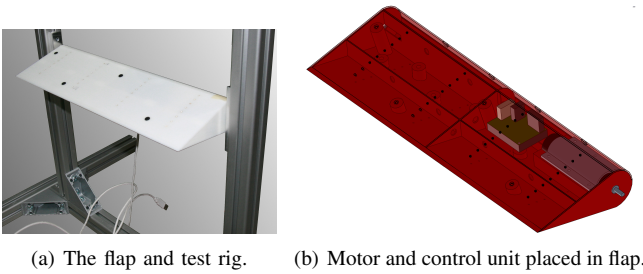

Fig. 4. Overview of the model.
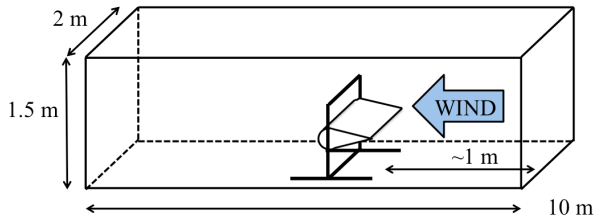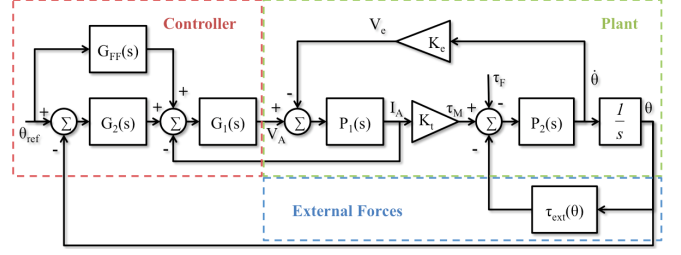
Hz and a maximal amplitude of $\pm 15°$, and with 2.4 Hz and $\pm 5°$ amplitude in Kobayashi's setup. We investigated a worst case scenario in terms of the flap's operating range and frequency, with movements of $\pm 30°$ at the motor's top speed and acceleration, when a step takes approximately 80 ms and corresponds to 6.25 Hz.

The experiments were carried out in a boundary layer wind tunnel (dimensions: 1.5x2x10m) with a top wind speed of 16 m/s. The test rig was placed near the inlet, as seen in Fig. 3.

III. MODEL DESIGN

Our aim is to capture the experimental setup with a model that is well anchored to the physical reality. A control system is typically represented by a controller and a plant, which in our case corresponds to the flap with the control unit and the motor mounted inside. Moreover, there are external forces that disturb our system, i.e. the gravity and the wind force. A schematic overview of the system is presented in Fig. 4.

The manufacturer provides a position control with a cascade structure with an inner PI current control loop, G_1, and an outer PID position control loop, G_2, and augmented by a speed and acceleration feed forward block, G_{FF}. The flap and the DC motor are modeled by the process blocks P_1, P_2, the back emf constant, K_e, and the motor torque constant, K_t. The external forces acting on the flap, gravity and wind, are assumed to be nonlinear functions of the flap angle and are modeled by the external torque block, τ_{ext}, in Fig. 4. The various parts of the model are represented in the frequency domain by Laplace transforms. In the following sections each part of the model is described in detail.

A. The Plant: DC Motor and Flap

The DC motor is modeled with an electrical part (P_1, K_e and K_t) and a mechanical part (P_2). The back emf voltage is proportional to the motor speed, $V_e = K_e\dot{\theta}$, and following Lenz's law is always counteracting the armature voltage, V_A. The resulting voltage generates the motor armature current, I_A, and is modeled by P_1. The electrical torque produced by the motor is proportional to the armature current, $\tau_M = K_t I_A$. The total mechanical torque (including losses) generates the motor speed and is modeled by P_2. The process blocks P_1 and P_2 are given by,

$$P_1(s) = \frac{1}{Ls + R} \qquad (1)$$

$$P_2(s) = \frac{1}{Js + b} \qquad (2)$$

(a) The flap and test rig.   (b) Motor and control unit placed in flap.

Fig. 2. Experimental setup

Fig. 3. The test rig placed inside the wind tunnel (not to scale).

where L is the motor inductance, R is the motor resistance, J is the rotor inertia, b is the viscous friction constant and s is the Laplace variable.

Mounting the motor in the flap increases the plant's inertia and friction (mechanical and air resistance). This is simply accounted for by adjusting the mechanical parameters (J and b) and by adding a constant friction, τ_F, as seen in Fig. 4.

B. PID Position Control

The motor position control is modeled by three parts: an inner current control loop, an outer position control loop, and a speed and acceleration feed forward,

$$G_1(s) = K_{P1} + \frac{1}{K_{I1}s} \tag{3}$$

$$G_2(s) = K_{P2} + \frac{1}{K_{I2}s} + \frac{K_{D2}s}{K_{D2}/(NK_{P2})s + 1} \tag{4}$$

$$G_{FF}(s) = \frac{1}{K_\omega s} + \frac{1}{K_\alpha s^2} \tag{5}$$

where K_{P1}, K_{I1}, K_{P2}, K_{I2}, K_{D2}, N, K_ω and K_α are the control parameters. All parameters except the filter coefficient N (predefined as 16) can be modified by the user.

Furthermore, the output of blocks G_1, G_2 are limited by 18 Volt and 3 Ampere, respectively. An anti-wind up method is implemented in order to avoid a growing integral part when the blocks are saturated. The details about the method the controller unit uses is not disclosed by the manufacturer; in our Matlab Simulink® model a conditional integration method (also called integrator clamping) is used [6].

C. Modeling External Forces

Gravity and wind are the external forces acting on the flap that are considered in our model. However, only the force components that are perpendicular to the flap's symmetry axis, as seen in Fig. 5, contribute to the motor torque. In the following sections the gravity and wind force models are described in detail.
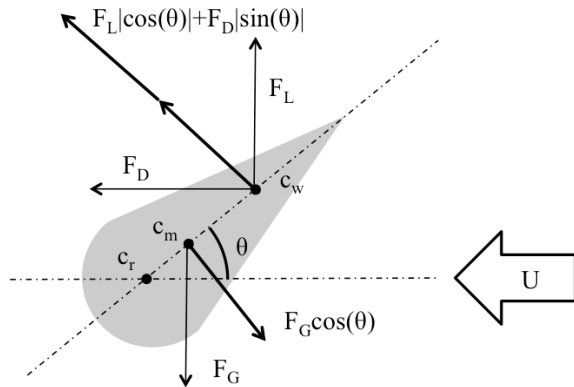

Fig. 5. External forces on the flap. The lift force, F_L, and the drag force, F_D, are functions of the wind speed, U. F_G is the gravity force. θ is the flap angle and c_r, c_m and c_w are the center of rotation, mass, and wind respectively.

1) Gravity Model: Since the flap's center of mass and axis of rotation are not aligned, the gravity will affect the motor torque. The gravity-induced torque τ_G is described by

$$\tau_G = r_G F_G cos(\theta) = r_G mg cos(\theta) \tag{6}$$

where m is the mass, g is the gravitational field acceleration (9.81 m/s^2), r_G is the distance between the flap's center of rotation and center of mass, and θ is the angle of the flap.

2) Wind Model: Assuming that the flap is flat (i.e. negligible thickness), the wind-induced torque τ_W is given by

$$\tau_W = r_W(F_L|cos(\theta)| + F_D|sin(\theta)|) \tag{7}$$

where F_L is the lift force, F_D is the drag force, r_W is the distance between the center of rotation (c_r) and the aerodynamic center (c_w), and θ is the flap's angle of attack. The aerodynamic center for a symmetric airfoil is typically located 1/4 of the chord length behind the leading edge and does not change position as the angle of attack does [8].

The drag and the lift forces are described by

$$F_D = \frac{1}{2}\rho U^2 C_D A \tag{8}$$

$$F_L = \frac{1}{2}\rho U^2 C_L A \tag{9}$$

where ρ is air density, U is the wind speed, A is the flap surface area, and C_D and C_L are the drag coefficient and lift coefficient, respectively.

The drag and lift coefficients depend on the object's shape, surface roughness, Reynolds number, and fluid properties. Changing the flap's angle of attack is essentially equivalent to changing the object's shape. Therefore, the coefficients are functions of the flap's angle of attack, $C_D(\theta)$ and $C_L(\theta)$.

The drag and lift coefficients for different angles of attack can be estimated experimentally; extensive experimental results are available from wind tunnel tests on National Advisory Committee for Aeronautics (NACA) standard airfoils. Sheldahl and Klimas present an experimental study of extracting the lift and drag coefficients of a series of symmetric NACA airfoils [7], with angles of attack ranging from 0° to 180°. Although our flap cannot exactly be classified as a NACA airfoil, it is symmetric and the measured drag and lift coefficients for the airfoil with the closest dimensions to our flap (with a 15% thickness-to-chord length ratio compared to 37% for our flap) are given in Fig. 6. The drag coefficient, in Fig. 6(a), is as one can expect maximized at 90° (vertical position) and zero at 0° and 180° (horizontal positions). In Fig. 6(b) the effect of stall on the lift coefficient can be seen at approximately 15°. When the airfoil stalls, the airflow separates from the back, the pressure drops and the lift decreases. The angle at which stall occurs depends on the airfoil shape, the fluid properties, and the Reynolds number.

Furthermore, $C_L(\theta)$ can be approximated by the theory of thin wings for small angles of attack. To summarize the theory, any arbitrary airfoil is assumed to behave like a thin plate, with a proportional relationship between the angle of attack and the lift coefficient as described in [8]:

$$C_L(\theta) = 2\pi\theta + C_{L0} \tag{10}$$
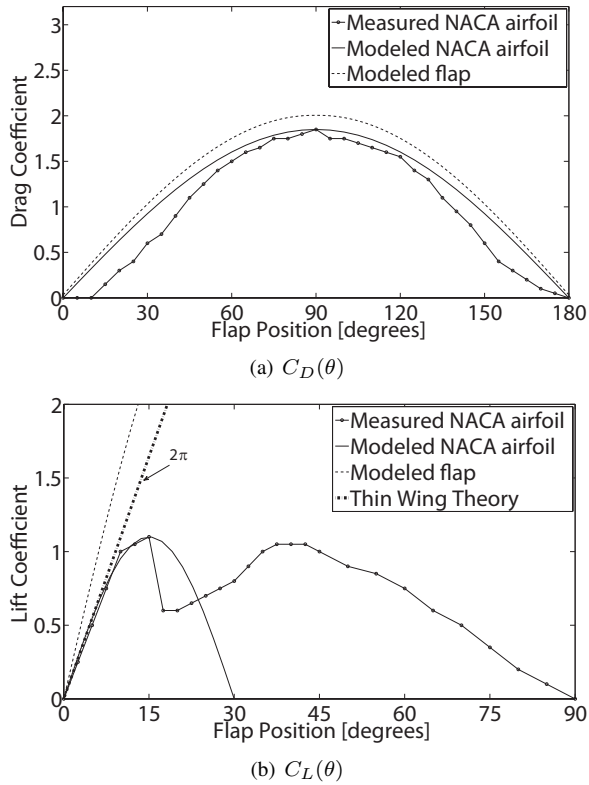
(a) $C_D(\theta)$

(b) $C_L(\theta)$

Fig. 6. Experimentally extracted $C_D(\theta)$ and $C_L(\theta)$ from a symmetric NACA airfoil [7]. The modeled flap curve is explained in section IV-C.

where θ is the angle of attack in radians and C_{L0} is the lift coefficient at $0°$. When the airfoil is symmetric there is no lift at $0°$, thus C_{L0} is zero. The proportional relationship in the stable region (before stall) between C_L and θ can be verified by looking at Fig. 6(b), where the NACA airfoil experimental results are reasonably well modeled (until $10°$ roughly) by the thin wing theory (10). However, since the operating range of our flap include larger angles, a better model is required. We propose a nonlinear model that also captures the attenuation of $C_L(\theta)$ when the flap stalls,

$$C_L(\theta) = C_{L\theta s} sin(\frac{\pi}{2\theta_s}\theta) \qquad (11)$$

where $C_{L\theta s}$ is the maximal lift coefficient, which occurs at the stall angle, θ_s. It is seen in Fig. 6(b) that the proposed model (11) applied to the NACA airfoil provides an improved lift model for large angles compared to the thin airfoil theory.

The drag coefficient can simply be approximated by

$$C_D(\theta) = C_{D90} sin(\theta) \qquad (12)$$

where C_{D90} is the drag coefficient at $90°$. The model (12) is compared to the measured NACA airfoil result in Fig. 6(a).

TABLE I

MODEL PARAMETER IDENTIFICATION

Parameter	Range	Estimation	Data Sheet
J [gcm^2]	9.5:0.1:11	9.9	9.49
b [μNms/rad]	0.5:0.1:1.5	1.0	0.87
τ_F[mNm]	0:0.02:0.12	0.1	-

IV. MODEL VALIDATION

The approach for experimental validation of the models described previously is detailed in the following sections.

A. Plant Model

The parameters for the DC motor model given in the data sheets were verified by comparing the model output and the measured output for the motor without flap or external forces.

However, the mechanical parameters J, b and τ_F need to be re-evaluated for the motor mounted in the flap. In order to avoid gravity interference with the parameter estimation the flap was placed vertically. Usually, b and τ_F are estimated by performing a series of constant speed experiments, when there is no acceleration and a linear relationship between the measured armature current and motor speed is obtained, as can be seen in (13). However, at high speeds, this method implies a flap movement of several rotations, an operation which is limited by cables in our test rig. Instead, we estimate all three parameters simultaneously with a series of position steps (varying the reference trajectories), where J, b and τ_F are tuned in order to minimize the Mean Square Error (MSE) between the measured and simulated position trajectories. Since the search space is small, a systematic parameter sweep (see Table I) sufficed for estimating these parameters.

$$K_t I_A - \tau_F - \tau_{ext} = \mathcal{L}^{-1}\left(\frac{\omega(s)}{P_2(s)}\right) = J\ddot{\theta} + b\dot{\theta} \qquad (13)$$

B. Gravity Model

The motor torque can be calculated from the measured armature current, as $\tau_M = K_t I_A$. While holding a static position, the motor torque is counteracting the external torque applied to the flap. The gravity torque can thus indirectly be measured when there is no wind force applied. The motor torque was measured at different flap angles (1536 samples taken at each position). The model parameters m and r_G were extracted from the Computer Aided Design (CAD) model of the flap. The mass of the motor and control unit was not considered since their center of mass is aligned with the flap's center of rotation.

The result from the static position measurements is compared to the gravity model described by (6) in Fig. 7. The measured gravity torque is slightly asymmetric and noisy. The asymmetry might be due to the fact that the weight is not evenly distributed along the symmetry axis of the flap (top and down), or possibly due to asymmetries of the motor. However, the gravity model was not further developed, since the asymetry effect is insignificant within the considered operating range ($\pm30°$), and the noise was ignored due to its negligible effect on the highly repeatable dynamic step responses (see Subsection IV-D).

C. Wind Model

The wind model was validated following the same experimental procedure as for the gravity model. The motor torque was measured at the same static angles, while the flap was under maximum wind load (16 m/s). The measured motor torque then counteracts the combined effect of gravity, lift,
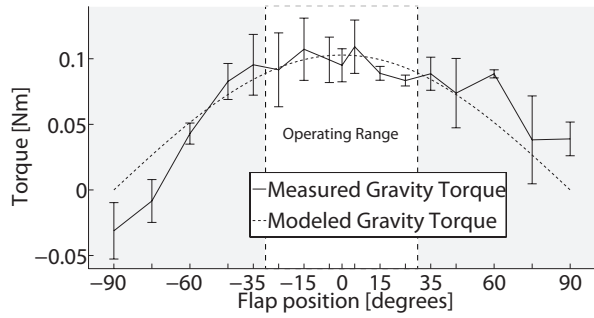
Fig. 7. Measured and modeled gravity torque, τ_G, as a function of the angle of attack, θ. The error bars represent the standard deviation.
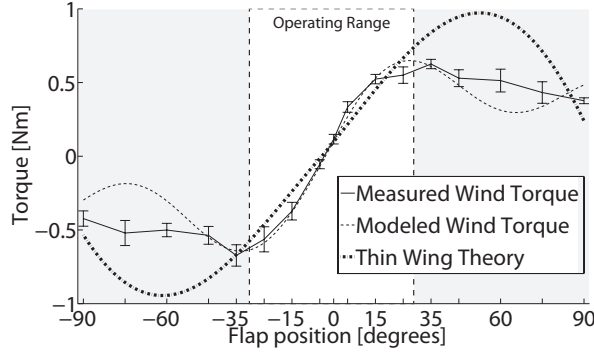

Fig. 8. Measured and modeled wind torque ($C_L(\theta)$ modeled by (11) or thin wing theory), τ_W, as a function of the angle of attack, θ. The error bars represent the standard deviation.

and drag. The combined wind torque (lift and drag) was obtained by subtracting the mean measured gravity torque from the measured motor torque, and is presented in Fig. 8. Note that the flap stalls at approximately $\pm 30°$.

The drag and lift coefficients, $C_D(\theta)$ and $C_L(\theta)$ cannot directly be estimated from the combined wind torque. Except at a $90°$ angle, where there is only drag and no lift present, which allows C_{D90} in (12) to be estimated (to 2.0). Furthermore, by leveraging the drag coefficient model, $C_{L\theta s}$ in (11) can be estimated (to 2.9) from the measured wind torque at the stall angle. The resulting models of $C_D(\theta)$ and $C_L(\theta)$ for the flap are seen in Fig. 6(a) and Fig. 6(b) respectively.

The resulting wind torque models, from applying both the thin wing theory and our proposed lift coefficient model, are presented in Fig. 8. Even at small angles the thin wing theory does not capture the wind torque particularly well. This is not surprising since the approximation is stronger for the flap (larger thickness-to-chord ratio) compared to the airfoil. However, our wind model for the flap is validated within, and slightly beyond, the operating range.

D. Overall System Model

In order to validate the dynamic model, presented in Section III (see Fig. 4), experimental data from position step responses at different wind speeds were compared with the model output. Note that the outcome of these steps, presented in Fig. 9, is highly repeatable in any wind condition. The same control parameters were implemented
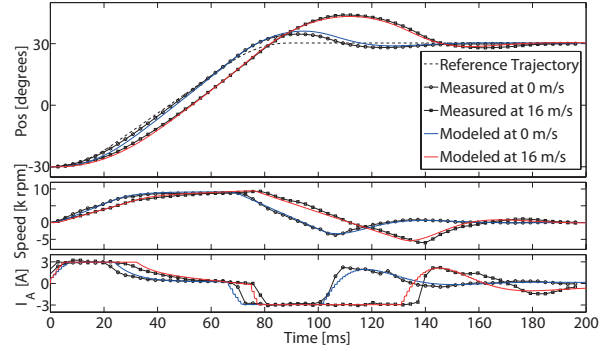

Fig. 9. Comparison of measured and simulated position steps of the flap at wind speeds of 0 m/s and 16 m/s.

on the physical and simulated control unit, and were set by the manufacturer's auto-tuning function. It is clear that the Matlab Simulink® model is able to capture the flap dynamics and the wind effect.

V. TUNING CONTROL PARAMETERS

The flap position should ideally follow the reference trajectory closely. However, as seen in Fig. 9, this is not the case: even without wind there is a noticeable overshoot. Therefore, we performed an offline optimization of the control parameters in our developed system model.

K_{P1}, K_{I1}, K_{P2}, K_{I2}, K_{D2}, K_ω and K_α are the control parameters that can be tuned. However, not all of them have the same impact in terms of overall system performance. For instance, the current control parameters (K_{P1} and K_{I1}) are already well tuned by the auto-tuning and further optimization has only a minimal effect. Moreover, the speed feed forward, K_ω, was set to zero by the auto-tuning function, and our simulation confirms that increasing it only has a negative effect on the system performance. In the end, the following control parameters were tuned: K_{P2}, K_{I2}, K_{D2} and K_α.

Appropriate control parameter ranges were chosen manually (in simulation), and are presented in Table II. The boundaries were chosen to avoid unstable regions or saturation effects. The increments were set as large as possible, while maintaining an insignificant effect on the performance.

A systematic parameter sweep was made, with the MSE between the actual (simulated) position and the reference position as tuning criterion. The parameters were tuned for two wind speeds, 0 and 16 m/s, and the identified control parameters for the two scenarios are presented in Table II.

The control parameters identified by the auto-tuning and the model-based tuning were validated with our experimental

TABLE II
CONTROL PARAMETER TUNING

| Parameter	Range	Auto-tuning	Model-based 0 m/s	Model-based 16 m/s
K_{P2}	100:25:500	148	325	400
K_{I2}	100:25:800	667	600	300
K_{D2}	150:25:600	176	325	400
K_α	25:25:250	23	100	250

TABLE III
CONTROL PERFORMANCE STATISTICS

Scenario		Overshoot [%]			Reference Trajectory [°] MSE		
		Auto-tuned 0m/s	Model-based 0m/s	Model-based 16m/s	Auto-tuned 0m/s	Model-based 0m/s	Model-based 16m/s
0 m/s	mean	7.5	0.8	0.5	4.0	0.5	0.4
	std	0.08	0.04	0.04	0.1	0.02	0.02
16 m/s	mean	23.6	18.5	13.6	48.5	29.6	20.0
	std	0.22	0.22	0.28	0.95	0.64	0.56
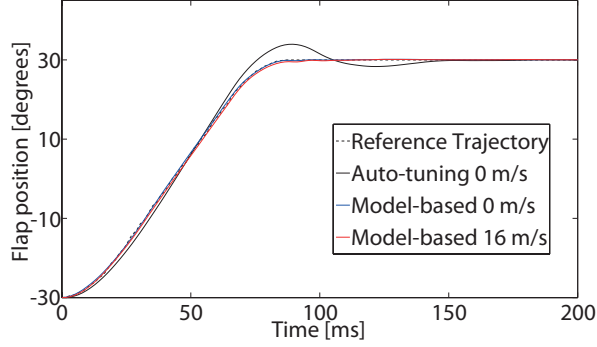
(a) Step response performed without wind.
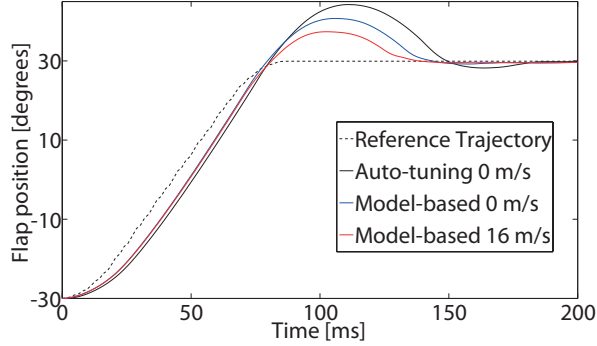
(b) Step response performed with a wind speed of 16m/s.

Fig. 10. Measured data from position steps, comparing the auto-tuning and model-based tuning system performance.

setup in the wind tunnel. Ten step responses of 60° were performed, both with and without wind, and for all three sets of control parameters (60 steps in total). Statistical results of these experiments are presented in Table III. Note that the parameters tuned in the harshest environment worked well for all scenarios, while the parameters found for the case without wind did not perform as well for experiments with wind. Furthermore, the model-based tuning, in any wind condition, but especially without wind, performs significantly better than the auto-tuning. This is also evident in Fig. 10, where a qualitative representation of the result is presented.

VI. CONCLUSIONS

In this paper, we proposed and validated a physically grounded model for a flap system operating in diverse wind conditions. We used this model to design and optimize a linear control law for the position of the flap. While in this paper we focused exclusively on the position control, the proposed model is detailed enough to allow tuning of control laws concerned with speed and torque.

The emphasis of this work has been on validating the model, while the tuning approach of the control parameters was crude and only to the point of showing a valid result. However, we showed that a parameter tuning based on our model outperforms the auto-tuning function provided by the manufacturer. Moreover, although more sophisticated optimization algorithms could be used, we are approaching the performance limit of the linear control, possibly also the physical limits of the motor, for this application.

Finally, the results indicate that little or nothing is gained by varying the control parameters depending on the wind speed. Control parameters tuned for the harshest conditions, maximal wind speed in our case, perform very well also for lower wind speeds within the desired range of operation.

In the near future, we will build our active bridge model, which will allow us to properly determine the flap requirements when operating as an array anchored to a structure.

REFERENCES

[1] A. Larsen, "Aerodynamics of Large Bridges", Taylor & Francis, 1992.

[2] H. Kobayashi and H. Nagaoka, "Active control of flutter of a suspension bridge", Journal of Wind Engineering and Industrial Aerodynamics, vol. 41, pp. 143-151, 1992.

[3] H. I. Hansen and P. Thoft-Christensen, "Active Vibration Control of Long Suspension Bridges", PhD Thesis, Dept. of Building Technology and Structural Engineering, Aalborg University, 1998.

[4] T. Theodorsen and I. E. Garrick, "Nonstationary flow about a wing-aileron-tab combination including aerodynamic balance NACA Rep. 736", N. A. C. f. Aeronautics, Ed., ed. Washington D.C., US, 1943.

[5] J.M. Fowler and R. D'Andrea, "A formation flight experiment", IEEE Control Systems Magazine, vol.23, no.5, pp.35-43, Oct. 2003.

[6] A. Visioli, "Practical PID control", Springer, 2006.

[7] E. R. Sheldahl, C. P. Klimas. "Aerodynamic Characteristics of Seven Symmetrical Airfoil Sections Through 180-Degree Angle of Attack for Use in Aerodynamic Analysis of Vertical Axis Wind Turbines", Albuquerque, NM 87185, Aerothermodynamics Division 5633, Advanced Energy Projects Division 4715, Sandia National Laboratories, 1981.

[8] I. H. Abbott and A. E. von Doenhoff, "Theory of Wing Sections: Including a Summary of Airfoil Data", Dover Publications, 1959.